Physics – Uspekhi **51** (11) 1161 – 1169 (2008)

PHYSICS OF OUR DAYS

PACS numbers: **42.30.–d**, **42.79.–e**, 87.64.Rr

Superresolution and singularities in phase images

V P Tychinsky

DOI: 10.1070/PU2008v051n11ABEH006682

Contents

1. Introduction	**1161**
2. Phase object model	**1163**
3. Singularities and the resolution criterion in phase images	**1163**
4. Singularities and wavefront dislocations in phase images	**1164**
5. Spatial resolution in dynamic phase images	**1166**
6. Singularities and superresolution in phase images	**1167**
7. Conclusion	**1168**
References	**1169**

Abstract. The Rayleigh criterion and the Airy radius r_0 are not adequate for characterizing spatial resolution in phase and some other functional images. An essential feature of phase images is a possible formation of wavefront dislocations which depend on the position in space of the so-called singular lines $[I(x, y, z) = 0]$, in the neighborhood of which the phase gradient grad $\varphi \approx I^{-1/2}$ increases and the intensity tends to zero. Based on this gradient phase behavior, the minimal length L dependent on the signal-to-noise ratio (S/N) is proposed as the phase resolution criterion, and a formula for the energy-dependent super-resolution, $\Xi = r_0/L \cong 2(S/N)^{1/2}$, is devised. Measurements on a 100-nm-diameter latex sphere using the Airyscan coherent phase microscope confirmed that a marked ($\Xi \cong 5$) superresolution can be achieved.

1. Introduction

The problem of resolution in optics has a long history and comes to our attention again with the advent of new methods in the microscopy of biological objects, taking advantage of the properties of functional images [1]. The Rayleigh resolution criterion based on intensity distribution in a point source image is actually a characteristic of the numerical aperture of an optical system [2] and cannot be applied to functional images such as fluorescent and spectral [3 – 9], holographic [10], interference [11 – 17], polarization and some other images.

Publications reporting superresolution on the order of dozens of nanometers in biological images [3 – 9] evoked a wide response. The possibility of detecting single macromolecules [4] and measuring their coordinates with nanometer accuracy [6] was demonstrated. These outstanding results were obtained containing devices with ordinary optics using nanocrystal quantum dots [3], fluorescent markers with different spectra [6], and photoactivatable proteins [4] to tag biological objects, taking into account substrate effects on fluorescence [7] and the suppression of protein fluorescence in structured illumination conditions [8]. One of these methods (termed as a stimulated emission depletion, STED) is based on the effect of reversible saturation of radiative transition. The minimal lateral dimension of the region in which the 'response' is recorded is on the order of $\Delta x \approx \lambda(\xi)^{-1/2}/\pi$, where $\xi \gg 1$ is the saturation parameter of transition related to photoinduced fluorescence. The use of optical astigmatism permitted determining the coordinates of individual fluorophores in three dimensions with a nanometer accuracy [9].

It follows from the cited studies [3 – 9] that the application of fluorescence methods in the microscopy of biological specimens yields data of great scientific and practical importance, on the one hand, and leads to the erosion of boundaries between general notions of spatial resolution and the accuracy of coordinate measurement, on the other hand.

The same studies showed that spatial resolution (including superresolution) depends not only on the numerical aperture but also on the properties of an object, algorithms of measurement and treatment of functional images, time of measurement, and signal-to-noise ratio. Hence, the natural question: Is it possible to exactly define the notion of superresolution in functional images generally, and in fluorescence and phase ones specifically? This question involves fundamental notions of physics; therefore, we believe it warrants a special discussion.

Interference methods are also extensively used in microscopy [11 – 17] by virtue of their low-invasive nature and feasibility of being employed to examine unstained natural objects. Their application to the microscopy of biological specimens makes it possible to obtain digital phase images, measure indices of refraction [13, 16], and record dynamic processes in real time and with a high responsivity [14 – 16]. However, algorithms for generating phase images, based on phase retrieval from interference patterns [11 – 17], did not

V P Tychinsky Moscow State Institute of Radio Engineering, Electronics and Automatics,
prosp. Vernadskogo 78, 119454 Moscow, Russian Federation
Tel. (7-495) 434 67 92
E-mail: vtych@yandex.ru

Received 8 June 2008, revised 29 August 2008
Uspekhi Fizicheskikh Nauk **178** (11) 1205 – 1214 (2008)
DOI: 10.3367/UFNr.0178.200811c.1205
Translated by Yu V Morozov; edited by A Radzig

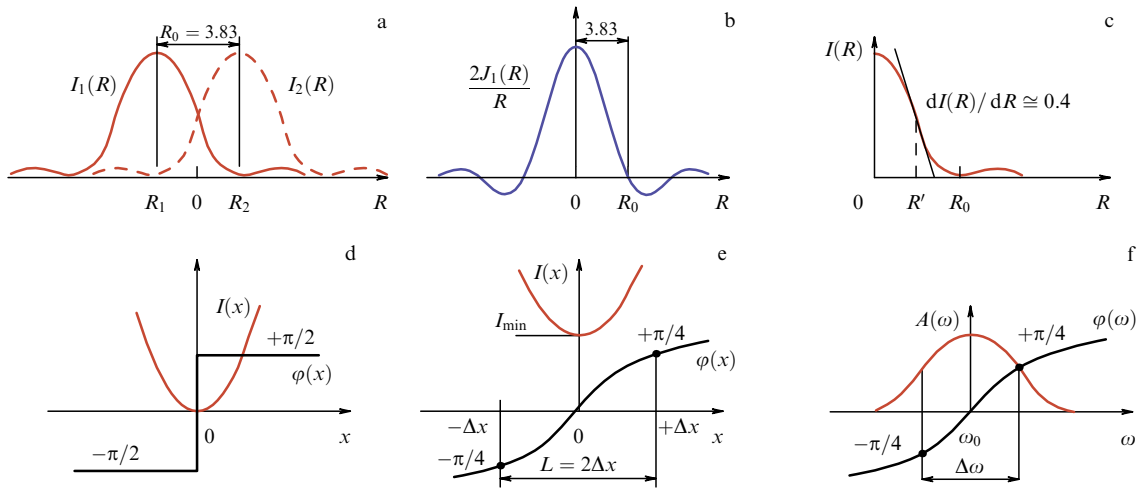

Figure 1. Spatial resolution in amplitude images and in the vicinity of a singular point. (a) Classical Rayleigh criterion — the distance between maxima in the images of two incoherent point sources — is $R_0 = 3.83$, where $R = 2\pi Dr/\lambda F = Kr$ is a dimensionless coordinate in the image plane. (b) Instrument function of the pupil of the optical system with the normalized Airy disk radius $R_0 = 3.83$. (c) Limited maximum intensity gradient in the vicinity of a point source. (d) Zero intensity at the singular point $x = 0$; π-jump of the phase occurs upon its intersection. (e) Quadratic change in intensity and a finite value of the phase gradient in the singular point neighborhood; distance $L = 2\Delta x$ between the points $\varphi(\pm\Delta x) = \pm\pi/4$ is used below as the resolution parameter in phase images. (f) Analogy with the phase-frequency characteristic $\varphi(\omega)$ of the oscillatory circuit; frequency band $\Delta\omega$ can be found from both the amplitude-frequency $[A(\omega)]$ and phase-frequency $[\varphi(\omega)]$ characteristics.

permit achieving superresolution registered in fluorescence images.

This paper focuses on the problem of superresolution in phase images, which is related to their unique properties usually interpreted in terms of so-called singular optics [18–26]. The notions of wavefront dislocations (WFDs) and singular lines at which the intensity goes to zero were introduced into optics in a fundamental work by J F Nye and M V Berry [18] dated 1974. Later other researchers defined such unusual notions as the birth and annihilation of singular points, the nature of screw dislocations, and topological charge value [19, 24]. Singular points are apparent only in interference images after phase retrieval (in phase images). Experimental and theoretical studies [19–26] in this relatively new branch of optics have provided a deeper insight into the structure of the optical field. Of fundamental importance is the inference [18, 22, 23] that an assembly of singular lines makes up a sort of 'skeleton' of an electromagnetic field and that an object image can be regarded as a projection of the 'skeleton'.

Wavefront dislocations inside the Airy disk were first observed [25, 26] in phase images obtained by coherent phase microscopy. However, dislocations were not discussed in later works on interference microscopy [10–17], in which other algorithms (e.g., multistep ones [17]) were utilized to obtain phase images.

The paramount importance of the algorithm and method for the production of phase images became evident after the first reports on superresolution [27, 28] had been published in 1989. Indeed, the absence of superresolution in phase images obtained by optical tomography [11], multistep interferometry [17], and holographic [13] and Hilbert phase [14–16] microscopies could be due to nothing more than the employment of algorithms based on recording intensity distribution. In these methods, interference images stored in computer memory were used to calculate the argument (phase) of the complex amplitude of a wave scattered by an object and to represent subsequently the phase (or the optical path difference) on the monitor in the form of a two-dimensional distribution. The intensity distributions in interference images being limited by diffraction by the objective aperture, we believe it to have excluded the possibility of superresolution in phase images.

A radically different algorithm was employed in the Airyscan coherent phase microscope developed in our laboratory [29, 30]. The optical path difference between the object and reference waves was measured in each pixel of the raster by a compensation method during sequential scanning of interference images. In this approach, the two-dimensional distribution of the optical path difference normalized to the wavelength was interpreted as the object's phase image $\varphi(x, y)$. Images of test-objects were found to exhibit superresolution [27–30]. At that time, we thought this superresolution to be an inherent property of phase images and did not care to seek a more adequate physical explanation of this phenomenon.

In what follows, it will be shown that the possibility of occurring superresolution in phase images follows from the well-known findings in classical [2] and singular [18–26] optics. We shall utilize the known intensity distribution in a point source image, which is limited by diffraction on the aperture of the optical system. This distribution may be represented by the function $I(R) = [(2J_1(R)/R]^2$, where $R = 2\pi Dr/\lambda F = Kr$, $K = 2\pi D/\lambda F = R_0/r_0 = 3.82/r_0$, where $r_0 = 0.61\lambda F/D$ is the Airy disk radius, D, F, λ are the aperture diameter, focal distance, and wavelength, respectively, and $r = (x^2 + y^2)^{1/2}$ is the distance in the image plane.

A physical model of the Rayleigh criterion comprises two identical incoherent point sources whose image is constrained by diffraction on the aperture of the optical system (Fig. 1a) or by the normalized Airy disk radius $R_0 = 3.82$ (Fig. 1b).

The normalized distance $R_0 = 3.82$ between extrema in the intensity distribution function $I(R) = [2J_1(R)/R]^2$ of two identical point sources (Fig. 1a) serves as the Rayleigh resolution criterion [2] and is numerically equal to the argument ($R_0 = 3.82$) for the second zero, $J_1(R_0) = 0$, of the

Bessel function of the first kind. The Rayleigh criterion is an equivalent of numerical aperture $\mathrm{NA} = D/F$ up to a wavelength λ. It is independent of energy and may be correctly applied only to two identical incoherent sources.

The model of two point sources shown in Fig. 1a can be converted into a simple model of a functional image with 'superresolution'. The latter proves to be energy-dependent and limited by the accuracy with which coordinates of the sources can be determined. To this end, suffice it to assume that the point sources with coordinates R_1 and R_2 in Fig. 1a differ, say, by spectral characteristics, their intensity distributions $I_1(R)$ and $I_2(R)$ are measured independently, and matched optical filters are used in the photodetector. The coordinates of either source can be determined under these conditions. Statistical error δR in the determination of the coordinates of each source depends on a matching between the spectra of the sources and the optical filters, the sensitivity of the photodetector, the number of independent realizations, and other factors formally characterized by the signal-to-noise ratio (S/N). The source images having been matched, the statistically significant distance ($\Delta R \approx 2\delta R$) between the centers of their Airy disks depends on the accuracy of measurements; in other words, it is energy-dependent in the above sense. In this functional image, the notion of superresolution can be formally defined as the $R_0/\Delta R \approx S/N$ ratio, but its meaning is far from obvious and the possibility of its application to other models remains to be elucidated. Even this example illustrates the necessity of a clearer definition of spatial resolution because the notions of resolution and accuracy of coordinate measurement are indistinguishable in certain functional images.

One more fundamental difference between the 'amplitude' image of a point source and its 'phase' analog needs to be emphasized. It follows from the definition of normalized intensity $I(R) = [2J_1(R)/R]^2$ in the image of a point source that the intensity gradient at its outskirts cannot surpass a certain ($\mathrm{d}I(R)/\mathrm{d}R \leqslant 0.4$) value (Fig. 1b). At the same time, in the case of a singular source with amplitude $J_1(R)$, the field at the point $R = 0$ changes its sign and the phase in the vicinity of $I(R) = 0$ undergoes a π-jump. This means that in phase images $\varphi(R)$ the phase gradient $\mathrm{d}\varphi/\mathrm{d}R$ at the intersection point between the singular line and the image plane is unlimited. Such phase π-jumps were regularly observed in the form of apparent $\lambda/2$-discontinuities (dislocations) of the surface in the images of different specimens [31–34] measured with the Airyscan microscope (see Section 6, Fig. 4).

The above example poses natural questions: "To what extent are functional (in particular, phase) images adequate to real objects?", and "What is the value of the information they contain?" Discussion of this nontrivial problem is beyond the scope of the present paper; suffice it to note here that numerous publications give positive answers to these questions and suggest a high informative value of functional images [3–16] obtained by new optical methods. This note is equally relevant with respect to images obtained by coherent phase microscopy [29, 31, 34, 35]. Also, very realistic phase images were produced in studies of subwavelength test-structures (slits and spheres) [27–29].

The primary objective of this paper is to attract attention to the problem of superresolution in phase images and to consider its relation to singular optics.

2. Phase object model

The electric field induced by a singular source, viz.

$$E(x, y) \approx J_1(R) \exp(\mathrm{i}\theta)\,, \tag{1}$$

where $J_1(R)$ is the Bessel function of the first kind, can be represented by a complex amplitude

$$\boldsymbol{E}(x, y) = E(x, y) \exp\left[\mathrm{i}\varphi(x, y)\right]\,,$$
$$\theta = \varphi(x, y) = \arctan\frac{x}{y}\,. \tag{2}$$

At the point $x = y = 0$, where singular line $\left[I(x, y, z) = 0\right]$ intersects the image plane Σ (see Section 4), the intensity is zero: $I(x, y) = |E(x, y)|^2 = 0$. Phase φ changes by 2π as it moves counterclockwise around the singular point.

Figure 1d shows quadratic growth of intensity $I(x)$ along the line $y = 0$ with distance from the singular point $x = y = 0$, and a π-jump of phase $\varphi(x)$ upon its intersection. The phase gradient is finite at points in the line $y \neq 0$ that does not pass through the singular point (Fig. 1e). Singular source model (2) and phase change $\varphi(x)$ in the neighborhood of the source will be used to substantiate the resolution criterion and the superresolution parameter constrained by the signal-to-noise ratio. Specifically, the linear size characterizing spatial resolution in a phase image (Section 3) will be taken as an interval $L = 2\Delta x$ between points with fixed phase values

$$\varphi(\pm\Delta x) = \pm\frac{\pi}{4}\,. \tag{3}$$

In connection with this definition of interval L, it is worth mentioning an interesting analogy between the processes in time and space. In radio engineering, the spectral resolution of temporal signals is evaluated from characteristics of the oscillatory LCR-circuit. The slope of its phase-frequency characteristic $\varphi(\omega) = \arctan[2(\omega - \omega_0)/\Delta\omega]$ grows in the vicinity of the resonance frequency ($\omega \cong \omega_0$) (see Fig 1f). At $\Delta\omega = 0$, phase $\varphi(\omega)$ at the point $\omega = \omega_0$ undergoes a π-jump. The frequency band $\Delta\omega$ characterizing spectral resolution can be defined at a level of $[A(\Delta\omega)]^2 = 1/2[A(\omega_0)]^2$ at the points $\omega - \omega_0 = \pm\Delta\omega/2$ of the amplitude-frequency characteristic $A(\omega)$ or from the points $\varphi_0 = \pm\pi/4$ of the phase-frequency characteristic $\varphi(\omega)$.

We shall use the above analogy and assume interval $L = 2\Delta x$ (Fig. 1e) between points with fixed values of $\varphi(\pm\Delta x) = \pm\pi/4$ to determine spatial resolution in the phase image $\varphi(x, y)$ of a singular source. This interval, $L = 2\Delta x$, is in a sense analogous to the frequency band $\Delta\omega$ in Fig. 1f. We shall demonstrate that the new criterion is energy-dependent unlike the classical Rayleigh criterion [2] that depends on optical system parameters alone.

3. Singularities and the resolution criterion in phase images

Suppose that two conjugate singular points A^+, A^- lie in the plane $\Sigma(x, y)$ of the object's image $\varphi(x, y)$ (Fig. 2), and the complex amplitude in the vicinity of one of them (A^-) is represented by expression (1) in the form

$$\boldsymbol{E}(R) = J_1(R) \exp(\mathrm{i}\varphi) \tag{4}$$

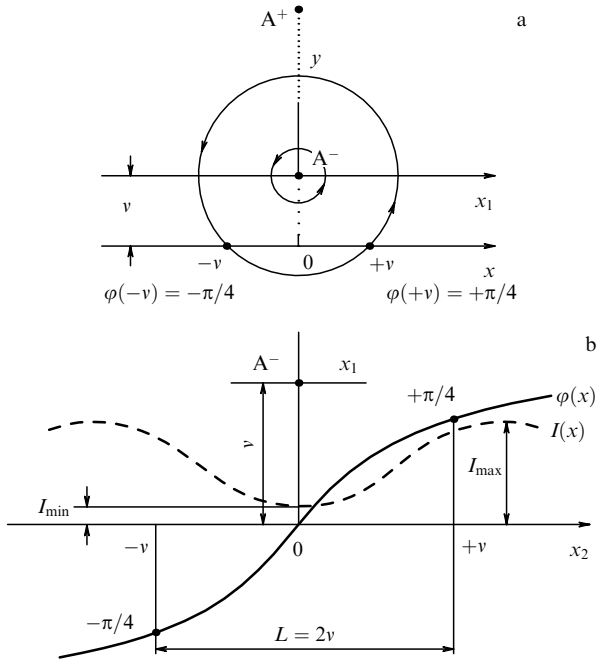

Figure 2. Model of a singular source in the image plane and definition of the spatial resolution criterion in a phase image. (a) A^+ and A^- are two conjugate singular points in the object's image plane (x, y). Singular point source $A^-(x_1 = y = 0)$ with a unit topological charge induces a field with the complex amplitude $E(x, y) = |E(x, y)| \exp[i\varphi(x, y)]$, where $E(x, y) \approx J_1(R) \exp[i\varphi(x, y)]$, $J_1(R)$ is the Bessel function, and the phase changes by 2π in detouring around the singular point. Intensity $I(x) = |E(x, y)|^2$ and phase $\varphi(x)$ of the field have finite values in the line $(x, y = v)$. At points $x = \pm v$, the phases differ by $\pi/2$. (b) Distance $L = 2v$ between the points $x = \pm v$ with phase values of $\pm\pi/4$ serves as the resolution criterion in the phase images. Minimal field intensity equaling the noise level $I_{\min}(0, v) = N$ limits the distance $L = 2v$. Maximum intensity $I_{\max}(0.5r_0) = 0.36$ occurs at the remote point $x \cong 2/K \cong 0.5r_0 > v$.

with the first zero at $R = 0$, the second zero at $R_0 = 3.82$, and the intermediate maximum at $R_2 \cong 2$. The phase in the neighborhood of the singular point $R = 0$ increases by 2π as it goes counterclockwise around the singular point [18–20].

At an arbitrary point with the coordinate x in line $y = v$ orthogonal to the segment A^+A^-, the intensity and the phase of the field created by the source A^- are represented by functions $I_\psi(x, v)$ and $\varphi(x, v)$, respectively. The phase

$$\varphi(x, v) = \arctan \frac{x}{v} \tag{5}$$

monotonically varies along the x-axis, and the intensity in the vicinity of the singular point ($R \ll 1$) changes with the square of the distance:

$$I_\psi(x, v) = \left[J_1(R)\right]^2 \cong \left(\frac{R}{2}\right)^2 = \frac{(Kr)^2}{4} = \frac{K^2(v^2 + x^2)}{4}. \tag{6}$$

The resolution criterion in phase images (Fig. 1e) is defined as a minimally discernible distance $L = 2v$ between the points $x = \pm v$, where the phase $\varphi_0 = \pm\pi/4$ (Fig. 2b). In this case, it is important that intensity $I_\psi(0, v)$ in formula (6) decreases as one approaches the singular point. This suggests that a minimal distance $v_{\min}$ at which a signal is still possible to measure at the points $x = \pm v_{\min}$ can occur. In real systems, this distance is limited by noise in the form of random intensity fluctuations caused by sources of different natures. The greater the signal versus noise, the smaller the values of interval $L = 2v_{\min}$ that can be measured.

Suppose further that the phase is measured at the point $x = v_{\min}$ at a certain minimal field intensity

$$I_\psi(v_{\min}) = \left[J_1(Kv_{\min})\right]^2 \approx \frac{K^2 v_{\min}^2}{2}, \tag{7}$$

limited by the noise level, with the nature of the noise being immaterial. Then, the highest field intensity $I_{\max} \cong 0.36$ occurs in an intermediate maximum ($R_2 \cong 2$) with the coordinate

$$r_2 \cong x_2 = \frac{2}{K} = \frac{\lambda F}{\pi D} \cong 0.5r_0 \gg v_{\min}. \tag{8}$$

The noise level ($S_{\min} = N$) is normally taken as a minimal signal level $S_{\min}$. In our notations at $S = I_{\max}$ and $N = S_{\min} = I_\psi(v_{\min})$, this corresponds to the condition

$$\frac{S}{N} = \frac{I_{\max}}{I_\psi(v_{\min})} = \frac{0.36}{I_\psi(v_{\min})}. \tag{9}$$

With account of relationship (7), it follows from Eqn (9) that

$$\frac{S}{N} \cong \frac{0.72}{(Kv_{\min})^2}, \tag{10}$$

or the final formula for the parameter Ξ of energy-dependent superresolution is given by

$$\Xi = \frac{r_0}{L} = \frac{r_0}{2v_{\min}} = \frac{1.9}{(0.72)^{1/2}} \left(\frac{S}{N}\right)^{1/2} \cong 2\left(\frac{S}{N}\right)^{1/2}. \tag{11}$$

This means that superresolution parameter Ξ in the model adopted is sufficiently 'universal' since it does not depend on phase object characteristics. In Sections 4 and 6 below, we shall consider the relation of resolution to singular lines and real phase images. Here, it is worth noting that the choice of the model is not a decisive factor. Indeed, formula (11) agrees up to a coefficient with the expression $w/L = (S/N)^{1/2}$ obtained earlier [25, 33] for the Gaussian beam model on the assumption of the equality between Airy and waist radii ($r_0 \cong w$).

4. Singularities and wavefront dislocations in phase images

A structured reflecting surface or a thin transparent optically weakly inhomogeneous object causes slight distortion (modulation) of the incident wavefront in coherent light and produces intensity $I(x, y)$ and phase $\varphi(x, y)$ distributions in the image plane of the optical system. By phase image is usually meant a two-dimensional distribution of the optical path difference (OPD) $h(x, y) = \varphi(x, y)\,\lambda/2\pi$ obtained with the help of an interference microscope. Let us suppose that a structured reflecting surface is represented by a geometric profile of height $Z(X, Y)$, where X, Y are the coordinates in the plane of an object. Then, the equality $Z(X, Y) \approx h(x, y)$ is satisfied up to a coordinate scale in the image plane xy of the object and with a limited accuracy in the profile reproduction [31]. In another case, for thin transparent objects, one finds in the approximation of geometric optics that

$$Z(X, Y) = \int n(X, Y, Z)\,\mathrm{d}Z \cong h(x, y), \tag{12}$$

where $n(X, Y, Z)$ is the refractive index distribution. The limited accuracy of the resemblance between the phase image represented by the OPD and the object $Z(X, Y) \approx h(x, y)$ is due to both fundamental (diffraction on the aperture, aberration) and technical (noise, limited responsivity, number of discretization levels, etc.) factors, detailed discussion of which is omitted here.

Of informative value in a phase image, as in other images, are structural elements and the position of their boundaries at which the phase gradient grows. As shown by theoretical and experimental studies in singular optics [19–26], the position of the boundaries depends on the structure of singular lines $I(x, y, z) = 0$ in the wave scattered by an object. Lines $I(x, y, z) = 0$ form a kind of field 'skeleton'; they are associated with the boundary conditions at the object's surface. Where the lines intersect the image plane Σ, the phase is not defined and undergoes a π-jump. If a singular line $I(x, y, z) = 0$ does not cross the plane Σ, then the intensity minimum and the enhanced phase gradient are observed at the points close to its projection. In this sense, amplitude $I(x, y)$ and phase $\varphi(x, y)$ images in the plane Σ can be regarded as a 'projection' of singular lines onto the image plane.

To illustrate such a dependence, Fig. 3a depicts projection AA of a singular line nn positioned at a distance of $v_1 < 0$ below the plane Σ. In the absence of intersections ($v_1 < 0$) between the singular line nn and the plane Σ, intensity $I(x, y)$ at all points of the plane becomes finite. The phase gradient grows at the point of intersection between the x-axis and projection line AA. It should be noted that changes in intensity $I(x)$ and phase $\varphi(x) = \arctan(x/v_1)$ shown earlier in Fig. 1e correspond just to this case. As optical inhomogeneity of the specimen increases, or due to other causes, the singular line $I(x, y, z)$ approaches the plane Σ. The phase gradient grows and intensity falls at the points close to projection AA. Finally, as the singular line intersects the image plane Σ, it acquires a pair of conjugate singular points (BB in Fig. 3b) and 'catastrophic' (in the mathematical sense) changes develop at the wavefront surface. As the singular points BB are detoured around in the direction shown by the arrows, the phase changes by 2π. The phase is continuous over the entire surface except for the segment BB, but the phase gradient grows unrestrictedly with approaching the singular points. In the image represented as surface $\varphi(x, y)$ there occurs a π-jump ('dislocation') at the BB segment (Fig. 4). It accounts for the disturbed conformity between the phase image $\varphi(x, y)$ and morphological parameters of the object, for example, structure of its surface $Z(X, Y)$. The number of singular points and the distance between them increase with increasing optical inhomogeneity of the object (Fig. 3c). When the number of singular points is large enough, there is no longer unambiguous correspondence between $\varphi(x, y)$ and the object in the so-called speckle images, and the informative value of the phase image is lost.

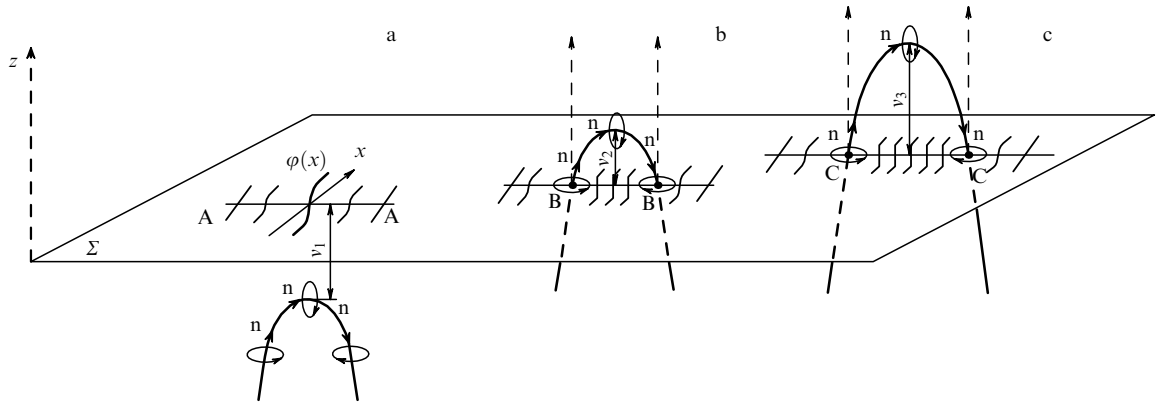

Figure 3. Dependence of the field structure in the image plane on singular line position v. (a) When singular line nn does not intersect image plane Σ ($v_1 < 0$), the local growth of the phase gradient $\varphi(x)$ occurs at points in line AA ('projections' of line nn). (b) At positive heights ($v_2 > 0$), the singular line nn intersects the image plane Σ at points BB. The phase gradient increases as one approaches the points BB, and the phase undergoes a π-jump as the points are intersected. Rings around singular points in the image plane Σ show the direction in which the phase grows. (c) The distance between singular points CC increases with height ($v_3 > v_2$). In phase images, the wavefront undergoes a $\lambda/2$-jump (dislocation) on the CC interval. A great number of singular points results in the loss of conformity between the image $\varphi(x, y)$ and the object.

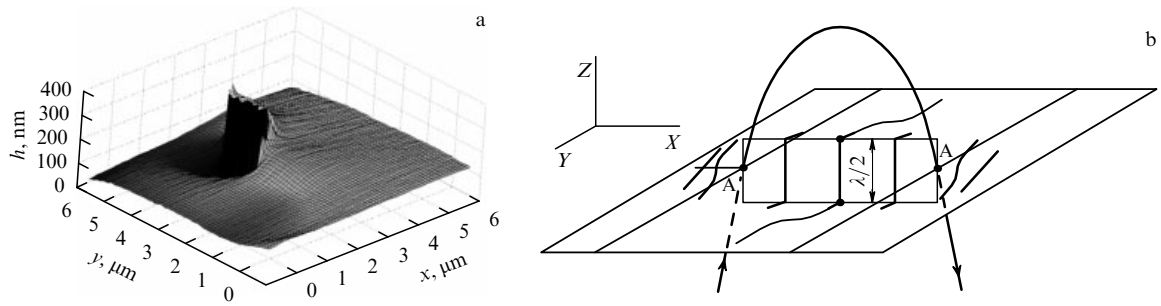

Figure 4. Dislocations cause distortion in phase images of objects. (a) 3D image of the nucleolus in an HCT116 cell with apparent surface discontinuity. (b) Interpretation of a $\lambda/2$-jump in the 3D image of the nucleolus caused by dislocation on the AA interval between singular points.

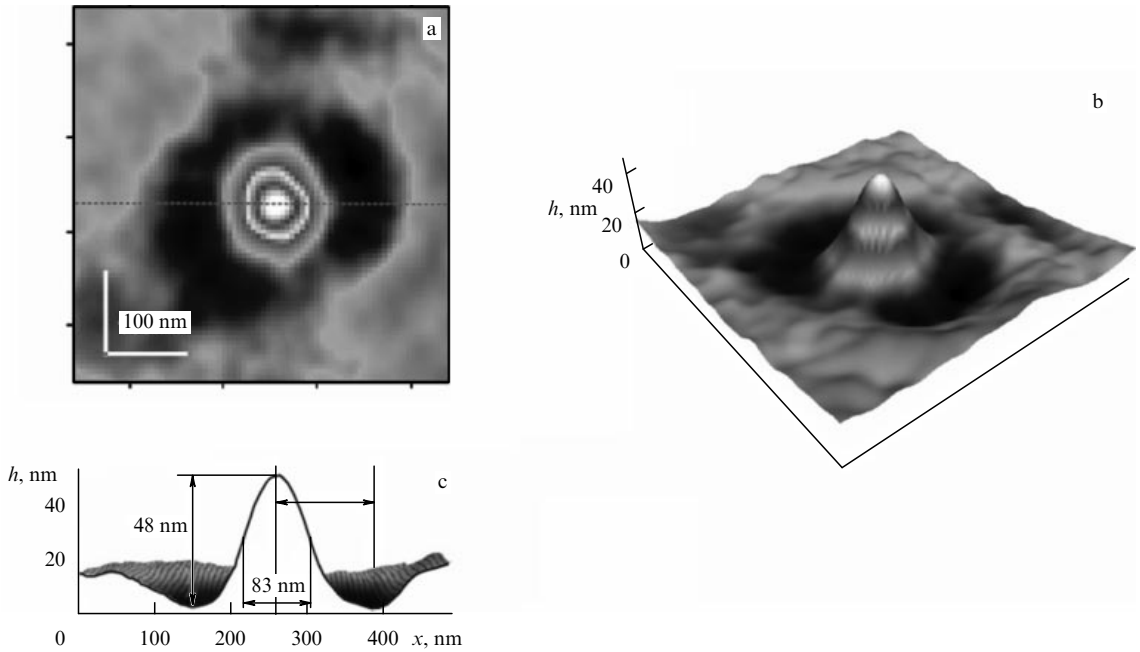

Figure 5. Phase image of a latex sphere 100 nm in diameter illustrates the possibility of attaining superresolution. Measurements were made with the Airyscan microscope having a 100/0.95 objective for which the Airy disk radius was $r_0 = 400$ nm. (a) Pseudocolor topogram $h(x, y)$. (b) 3D image of a sphere with shape distortions characteristic of diffraction. (c) Profile of diametral section through the topogram in which the phase thickness ($\Delta h = 48$ nm) and half-height diameter ($d = 83$ nm) were measured.

A rigorous phase image theory remains to be developed; hence, the importance of experimental and theoretical studies on singular optics that may explain the relationship between the skeleton and the field structure. Numerous works concerned with phase microscopy showed that in many cases (Fig. 5) the above factors do not interfere with obtaining quite plausible images of objects [10 – 16], realizing superresolution [27 – 30, 34, 35], or recording local dynamic processes [31, 34, 36].

5. Spatial resolution in dynamic phase images

It was mentioned in the Introduction that the accuracy of coordinate measurement in functional images is in some instances synonymous to spatial resolution. This remark equally holds for some dynamic phase objects. A simple example of a dynamic object is the moving boundary of a structural element. In such a case, the purpose of measurement may be to determine a minimal displacement of the boundary in the object's phase image plane.

It should be emphasized that natural factors limiting the possibility of registering minor displacements in the amplitude images of dynamic objects include small intensity gradient $\mathrm{d}I/\mathrm{d}R$ (Fig. 1c) at the boundary of a structural element and, as a rule, insufficiently large signal-to-noise ratio. Therefore, the minimal boundary displacement recorded from intensity variation is not normally at great variance with the Airy disk radius $r_0 = 0.61\lambda F/D$.

However, gradient $\mathrm{d}\varphi/\mathrm{d}R$ can be large in phase images, which facilitates recording small displacements. A dynamic object is exemplified by the model presented in Fig. 2a in which the singular source described by formula (2) moves along the x_1-axis. Its migration $x_1(t)$ at a fixed point with coordinate x in line $y = v$ causes changes in the field intensity and phase. These changes may be described by the following formulas, respectively:

$$I_\psi(t, x, v) \cong \frac{(Kr)^2}{4} = K^2\,\frac{v^2 + (x + x_1(t))^2}{4}\,,$$
$$\varphi(t, x, v) = \arctan\frac{x + x_1(t)}{v}\,. \tag{13}$$

At small displacement amplitudes ($\Delta x_1 \ll v$), the formulas for phase and intensity alterations assume the form

$$\Delta\varphi(t, x, v) = \frac{\mathrm{d}\varphi}{\mathrm{d}x}\,x_1(t) \cong \frac{x_1(t)}{v}\left[1 + \left(\frac{x}{v}\right)^2\right]^{-1},$$
$$I_\psi(x, v) \cong \frac{(Kr)^2}{4} \cong K^2\,\frac{v^2 + x^2}{4}\,. \tag{14}$$

Responsivity to source displacements will be highest at point $x = 0$ with maximum phase gradient $\mathrm{d}\varphi/\mathrm{d}x \cong 1/v$ and minimal intensity $I_\psi(v) = K^2 v^2/4$.

Let us suppose further that the source executes slow periodic motions with the amplitude Δx_1, which are accompanied by recording phase changes $\Delta\varphi(t, x, v)$. Then, the minimal measured amplitude Δx_1 will be limited by two factors, namely, the responsivity

$$\langle\varphi\rangle \cong \left(\frac{\Delta x_1}{v}\right)_{\min} \tag{15}$$

of the measuring device to phase changes (e.g., the number of discretization levels or phase noises), and the amplitude noise level at point $x = 0$:

$$S(x = 0) = I_\psi(v_{\min}) = K^2\,\frac{v_{\min}^2}{4} = N\,. \tag{16}$$

To recall, it follows from formula (9) that $S/N = I_{\max}/I_\psi(v_{\min}) = 0.36/I_\psi(v_{\min})$. Then, formulas (9) and (16)

give the expression for the minimal distance toward the singular point:

$$v_{\min} = 0.72\,\frac{(S/N)^{-1/2}}{K} = 0.19 r_0 \left(\frac{S}{N}\right)^{-1/2}. \qquad (17)$$

Taking into consideration the definition of responsivity (15), it is possible to derive from expression (17) a formula for the minimum displacement amplitude normalized to r_0:

$$\Xi^{-1} = \left(\frac{\Delta x_1}{r_0}\right)_{\min} \cong 0.19\langle\varphi\rangle \left(\frac{S}{N}\right)^{-1/2}. \qquad (18)$$

As the distance from the point of registration ($|x| \neq 0$) to the source increases, the minimal measured amplitude grows with the distance squared:

$$\Xi^{-1} = \left(\frac{\Delta x_1}{r_0}\right)_{x} \cong 0.19\langle\varphi\rangle \left[1 + \left(\frac{x}{v}\right)^2\right] \left(\frac{S}{N}\right)^{-1/2}. \qquad (19)$$

It can be seen from a comparison of formulas (11) and (18) that the responsivity to singular point movements in phase images may be very high. The results of measurements presented in Section 6 illustrate the possibility of recording very small amplitudes of the motion of a structural element boundary.

6. Singularities and superresolution in phase images

A comprehensive analysis of works and the current state of 'singular optics' is presented in Refs [18–26]. Notice that ordinary images have no singularities. Characteristic indications of singular points and dislocations are 'forks' or shifts in interference fringes, which are normally observed in interference images of phase transparents, either synthesized or natural, registered in coherent light. However, the dependence of the position of singular points (or WFDs) on the structure of microspecimens in the general case remains unknown. As mentioned earlier, dislocations regularly observed in images of relatively thick cells with the Airyscan coherent phase microscope used to be regarded as undesirable distortions hampering object identification.

Dislocation in the form of a $\lambda/2$-jump in phase thickness $h(x, y)$ characteristic of biological microobjects is shown for a human cell nucleolus in Fig. 4a. Apparent surface discontinuity of the nucleolus can be seen on the segment bounded by singular points. It should be noted that the character of dislocation and the distance between the singular points depend not only on object properties but also on the objective numerical aperture, focusing accuracy, and some other factors. Figure 4b offers an interpretation of the dislocation line as the projection of the singular line intersecting the image plane at the points AA.

Another example is presented to illustrate a completely adequate image of a subwave object and the possibility of attaining superresolution [29]. A characteristic topogram and 3D image of a latex sphere 100 nm in diameter are demonstrated in Fig. 5a, b. A profile of a diametral section through the topogram depicted in Fig. 5c evidences a distortion (presumably due to diffraction) and dimensions (half-height diameter, $d = 83$ nm, and maximum phase thickness, $\Delta h = 48$ nm). The lateral dimension, $d = 83$ nm, proves to be twice as small as the distance (≈ 140 nm) between the minimum and maximum values in the phase thickness profile and can be regarded (in the present case) as a characteristic of spatial resolution. Formally, this result can be interpreted as an illustration of five-fold superresolution $\Xi = r_0/d \cong 5$ in a phase image of a concrete test-object [29]. Measurements using an objective with NA = 0.95 at $\lambda = 633$ nm give the Airy disk radius $r_0 = 400$ nm. Notice also that if refractivity $\Delta n = n - 1 = \Delta h/d \cong 0.6$ is defined as the ratio of phase thickness to diameter [31], latex index of refraction $n = 1.6$ is very close to the real value of $n = 1.55$.

Interpretation of the measurement data for dynamic objects poses a much more complicated problem and cannot be totally unambiguous, inasmuch as there is no generally accepted terminology for them or resolution criterion. On the one hand, interference methods are known to be highly responsive (up to small fractions of a nanometer) to OPD variations in the axial direction. On the other hand, there are very few reports on the measurement of small tangential displacements and on the factors influencing its precision. It may be supposed based on general considerations that responsivity to tangential displacements is much lower because their minimal amplitudes are restricted not only by the signal-to-noise ratio but also by the degree of contrast at the boundary of a structural element in a moving object.

Measurement results from Ref. [32] are cited here to illustrate the possibility of attaining spatial 'superresolution' in a dynamic object image, bearing in mind the aforementioned conditionality of this notion. The test-object used in work [32] is the surface of a compact disk with a known microrelief structure. The phase height profile (Fig. 6a)

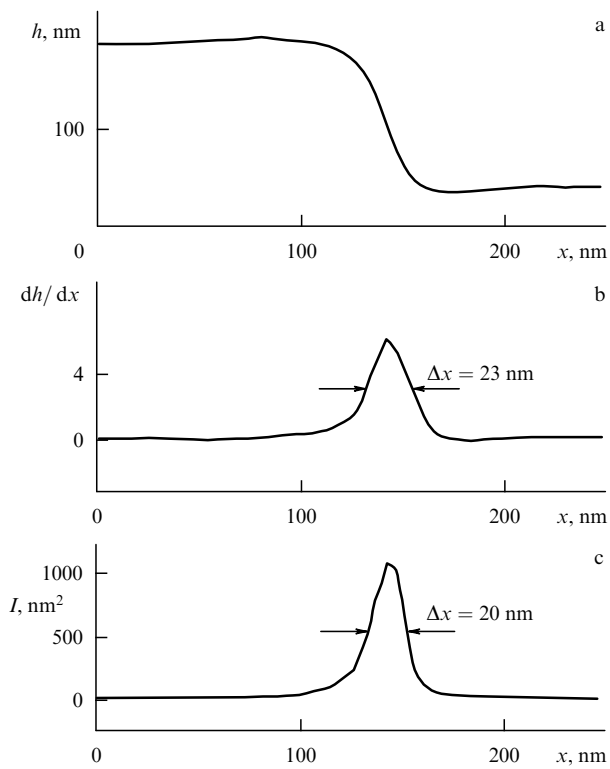

Figure 6. Local phase height fluctuations at the boundary of a structural element. (a) Fragment of the compact disk profile with a phase height difference of about 150 nm. (b) Determination of the exact ($\Delta x = 23$ nm) slope width by the $h(x)$-profile differentiation. (c) Illustration of the possibility of attaining 'superresolution' in phase images of dynamic objects. In the present case, the local ($\Delta x = 20$ nm) rise in the intensity $I(x)$ of phase height fluctuations at the profile slope is due to technical factors.

measured using an objective with NA = 0.95 shows a part of the protrusion with $\Delta h \cong 150$ nm and a 20 – 30-nm wide slope at its boundary. The slope width was determined more exactly ($\Delta x = 23$ nm) by the $h(x)$-profile differentiation (see Fig. 6b). Measurements of a large (≈ 300) series of phase height profiles were made by dynamic phase microscopy [31]. It was revealed that the height of profile $h(x)$ fluctuated within small fractions of a second, the main sources of fluctuations being various technical factors (unstable scanning, vibrations of the measuring device, and acoustic noises). The steep portion of the slope proved to be especially responsive to the fluctuations; this observation was confirmed by the position of their maximum intensity (I [nm^2]) (Fig. 6c). Phase height fluctuations were localized at a 20-nm-long steep part of the profile, close to the slope width $\Delta x = 23$ nm.

In this case, the boundary of the protrusion may be regarded as a 'dynamic' object undergoing weak chaotic movements, and the regions of local fluctuations in the phase image of the boundary in Fig. 6c as its fluctuation 'portrait'. Bearing in mind what was said about the conditionality of the terminology, this result can be interpreted as an illustration of achieving 20-fold ($\Xi = r_0/\Delta x = 17.5$) superresolution in the image of a dynamic object.

Moreover, it has concrete practical implications despite controversy around the definition of 'superresolution' because it explains causes for the rise in fluctuation intensity encountered in measurements of live biological objects [31]. Enhanced fluctuation intensity and the presence of contrast components in the spectra were regularly observed in the vicinity of steep portions of the phase thickness profile. The dependences of fluctuation spectra and intensities on inhibitors and stimulators suggested their relation to metabolic processes [31 – 35]. In certain cases, the region where fluctuations were localized ($\approx 50 - 100$ nm) turned out to be almost as wide as the profile, i.e., equal to a small fraction of the Airy radius. The local character of phase thickness fluctuations of the same order ($\Delta x \approx 50 - 100$ nm) was verified in biological specimens by the raster scanning technique [35]. Our measurements of dynamic objects [29 – 35] have led to an application-important conclusion about the possibility of recording very weak (a few angstroms) fluctuations of different natures at steep portions of the phase profile.

With regard to the results of measurements of a conventional dynamic object, presented in Fig. 6, metrologically more grounded measurements of an object undergoing controlled tangential displacements are of interest. In order to verify the method and to estimate limiting resolution, measurements were made on a dynamic object in the form of a narrow (≈ 200 nm) notch at the surface of a translator, periodic movements of which were controlled by an external voltage source [36]. The piezoeffect on a lithium niobate crystal was used for controlled tangential displacements in the Nanotester translator.

Figure 7 portrays two phase height profiles of notch with the maximum image profile steepness $S = \mathrm{d}h/\mathrm{d}x \approx 0.5$, offset by $\Delta x = 20$ nm in the plane by voltage applied to the crystal. Successive voltage reduction in time was accompanied by a decrease in the displacement amplitude. Voltage dependence of the displacement amplitude on a log-log scale is shown in Fig. 8. The minimal amplitude of periodic tangential movement at a frequency of 1 Hz in measuring for ≈ 200 s amounted to 0.06 nm [36]. The value of $\langle\varphi\rangle \approx 0.01$ rad obtained from formula (18) for $r_0 = 400$ nm agrees with that for $S/N \approx 100$.

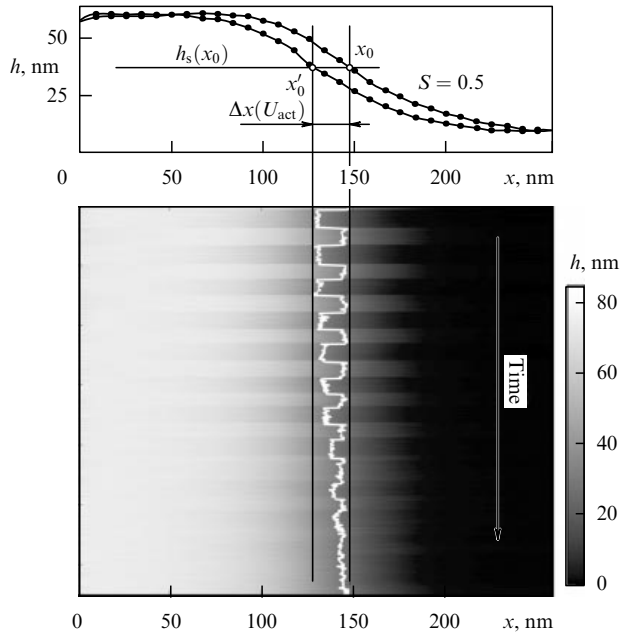

Figure 7. Measurements of the amplitude of controlled nanometer lateral displacements. Translational displacement ($\Delta x = 20$ nm) of a notch over the surface of a Nanotester piezotranslator [36] was brought about by applied voltage. Successive voltage reduction at the piezotranslator in time was accompanied by a decrease in the amplitude of the displacement of the structural element boundary.

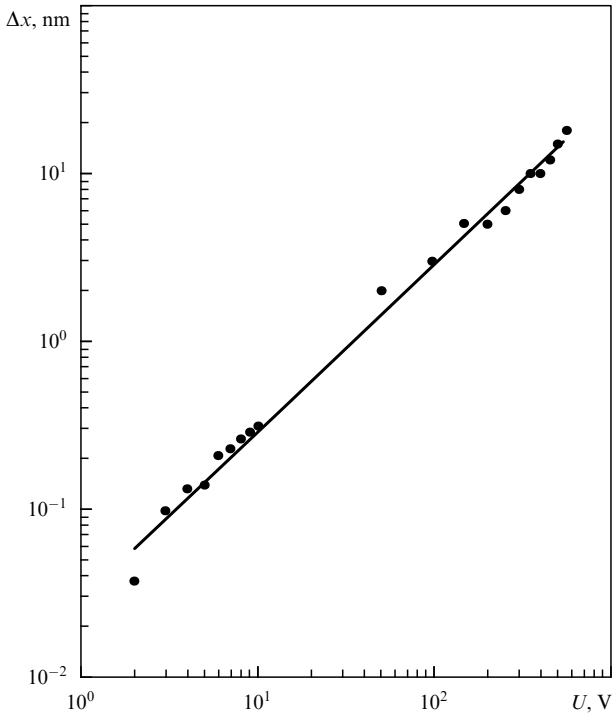

Figure 8. Measurements in a wide dynamic range showed the linear dependence of the displacement amplitude on the applied voltage [36]. Minimal measured amplitude reached 0.06 nm.

7. Conclusion

Extension of the notion of spatial resolution to functional images necessitated revision of the classical criterion and interpretation of the term 'superresolution'. We largely

confined ourselves to the discussion of methodical aspects in application to phase images. Their unique properties can be explained in terms of singular optics. Due to the lack of a rigorous phase image theory, we tentatively consider the model interpreting structures in a phase image as a 'trace' of 'hidden' singular lines (Fig. 3a) to be fairly demonstrative at the qualitative level.

The main result of this work consists in substantiation of the energy-dependent resolution criterion and measurements illustrating the possibility of attaining superresolution in phase images. In recent years, there has been growing interest in the phenomenon of superresolution in optics as related to biophysics, nanoengineering, and molecular medicine. To our knowledge, this important problem has been given surprisingly little attention in publications on interference microscopy [10 – 17]. One of the causes for this paradox appears to be the differences in phase measurement algorithms. The compensation method used in the Airyscan coherent phase microscope [29, 30] permitted realizing superresolution in phase images that was absent when measurements were made by other methods [10 – 17].

To conclude, a fundamental result of a general character for wave fields should be mentioned. It follows from formulas (14) and (16) for the phase gradient $\mathrm{d}\varphi/\mathrm{d}x \cong 1/v$ and intensity $I_\psi(v) = K^2 v^2/4$ that the relationship $\mathrm{d}\varphi/\mathrm{d}x \cong |\mathrm{grad}\varphi| \cong KI^{-1/2}/2$ is valid. This result can be generalized over the entire space and formulated as the 'uncertainty relation' for intensity and phase, meaning that phase uncertainty increases indefinitely with approaching lines with a zero field intensity.

Acknowledgments. The data included in the paper were obtained at the Laboratory of Coherent Optics, MIREA in 1987 – 2008. The author is gratefully acknowledge his colleagues who participated in the development of the Airyscan microscope: I Mazalov, D Ublinskii, and S Klushin. A Tavrov, G Kufal', E Perevedentseva, and T Vyshenskaya were involved in the study of phase images. A Kretushev greatly contributed to the development of mathematical support and to the improvement in instrument performance. Thanks are due to A Shtil', A Tikhonov, L Yaguzhinskii, I Vasilenko, and D Weiss for their fruitful cooperation. The work was supported by RFBR grant No. 07-04-00473.

References

1. Peng H *Bioinformatics* **24** 1827 (2008)
2. Born M, Wolf E *Principles of Optics* (Oxford: Pergamon Press, 1965)
3. Lacoste T et al. *Proc. Natl. Acad. Sci. USA* **97** 9461 (2000)
4. Betzig E et al. *Science* **313** 1642 (2006)
5. Bates M et al. *Science* **317** 1749 (2007)
6. Agrawal A et al. *Proc. Natl. Acad. Sci. USA* **105** 3298 (2008)
7. Wu D et al. *Nano Lett.* **8** 1159 (2008)
8. Hell S W *Phys. Lett. A* **326** 140 (2004)
9. Huang B et al. *Science* **319** 810 (2008)
10. Carl D et al. *Appl. Opt.* **43** 6536 (2004)
11. Vyshnyakov G et al. *Eur. J. Microsc. Analysis* **87** 19 (2004)
12. Langoju R, Patil A, Rastogi P *Opt. Express* **13** 7160 (2005)
13. Rappaz B et al. *Opt. Express* **13** 9361 (2005)
14. Popescu G et al. *J. Biomed. Opt.* **10** 060503 (2005)
15. Ikeda T et al. *Opt. Lett.* **30** 1165 (2005)
16. Popescu G et al. *Opt. Lett.* **31** 775 (2006)
17. Millerd J E et al. *Proc. SPIE* **5531** 304 (2004)
18. Nye J F, Berry M V *Proc. R. Soc. London A* **336** 165 (1974)
19. Bazhenov V Yu, Vasnetsov M V, Soskin M S *Pis'ma Zh. Eksp. Teor. Fiz.* **52** 1037 (1990) [*Sov. JETP Lett.* **52** 429 (1990)]
20. Berry M V, Dennis M R *Proc. R. Soc. London A* **457** 2251 (2001)
21. Leach J et al. *New J. Phys.* **7** 55 (2005)
22. Soskin M S, Vasnetsov M V "Singular Optics", in *Progress in Optics* Vol. 42 (Ed. E Wolf) (Amsterdam: North-Holland, 2001) p. 219
23. Baranova N B et al. *Pis'ma Zh. Eksp. Teor. Fiz.* **33** 206 (1981) [*JETP Lett.* **33** 195 (1981)]
24. Angelsky O V et al. *Phys. Rev. E* **65** 036602 (2002)
25. Tychinsky V *Opt. Commun.* **81** 131 (1991)
26. Tavrov A V, Tychinsky V P *Proc. SPIE* **2004** 332 (1994)
27. Tychinsky V P *Opt. Commun.* **74** 41 (1989)
28. Tychinskii V P et al. *Pis'ma Zh. Tekh. Fiz.* **17** (22) 80 (1991) [*Sov. Tech. Phys. Lett.* **17** 815 (1991)]
29. Tychinskii V P et al. *Kvantovaya Elektron.* **24** 754 (1997) [*Quantum Electron.* **27** 735 (1997)]
30. Tychinsky V P et al. *Opt. Commun.* **74** 37 (1989)
31. Tychinskii V P et al. *Usp. Fiz. Nauk* **177** 535 (2007) [*Phys. Usp.* **50** 513 (2007)]
32. Kretushev A V, Tychinskii V P *Kvantovaya Elektron.* **32** 66 (2002) [*Quantum Electron.* **32** 66 (2002)]
33. Tychinsky V P, Velzel C H F, in *Current Trends in Optics* (Ed. J C Dainty) (San Diego: Academic Press, 1994)
34. Tychinsky V P et al., in *Technical Proc. of the 2006 NSTI Nanotechnology Conf. and Trade Show, Boston, May 7 – 11, 2006* Vol. 2 (2006), Ch. 1, CD-ROM
35. Ivanov A B et al. *Ross. Nanotekhnol.* **2** (5 – 6) 120 (2007)
36. Tychinsky V P, Kretushev A V, Luskinovich P N, physics/0608093